Ductility analysis of vegetal-fiber reinforced raw earth concrete by mixture design

S. Imanzadeh, A. Jarno, A. Hibouche, A. Bouarar, S. Taibi

Ductility analysis of vegetal-fiber reinforced raw earth concrete by mixture design

S. Imanzadeh [a.b *], A. Jarno [b], A. Hibouche [b], A. Bouarar [b], S. Taibi [b]

[a] Normandie Univ., INSA Rouen Normandie, Laboratoire de Mécanique de Normandie, 76801 Saint-Etienne du Rouvray, France

[b] Normandie Univ., UNIHAVRE, CNRS, LOMC, 76600 Le Havre, France

* Corresponding author (saber.imanzadeh@insa-rouen.fr)

Abstract: Building construction technology by raw earth materials is already known and used since ancient times. The raw earth material is abundant, low cost, requires very low energy to manufacture and does not generate waste. Ductility is required for earth building materials in the areas of seismic risks where the earth buildings are particularly vulnerable to earthquakes. Hence, a raw earth treatment by binders and vegetal fibers is one of the techniques applied to improve its strength and ductility. This paper presents the use of mixture design as a tool to evaluate and analyze the plastic behavior of the raw earth material. The ductility is quantified through two ductility indices. The results indicate that an alternative ductility index based on the post-peak behavior of the material could be used to define a ductility criterion to meet specific requirements of the seismic regions.

Key words: Raw earth material, Flax fibers, Workability, Design Of Experiments, Mixture design, Ductility, Post-peak behavior

1. Introduction

The raw earth-based materials have been the subject of renewed interest in the recent years with the search for alternative building materials, *i.e.* ecological and economical materials. The main advantages of these materials are their low consuming energy for production, their availability in the large quantity, their recyclability, their low-cost construction and their easy in-situ implementation ([1], [2], [3], [4]). Therefore, they are suitable even in impoverished areas. Numerous studies have been dedicated for improvement of the mechanical and hygrothermal natural properties of raw earth material [5]. Therefore, raw earth constitutes a matrix where various components - natural or/and manmade materials - are added to reinforce one particular property. According to the used raw earth construction technique, the compressive strength could be improved in order to be used as a construction and building material. This improvement can be achieved by adding low quantity of binders such as lime and cement and sometimes adding fibers. Recent studies have demonstrated the influence of these binders on the raw earth material properties ([5], [6], [7], [8]). In particular, cement is known to be effective for improving the material strength. For example, Delgado and Guerrero [9], in a review paper on earth construction in Spain, provided the compressive strength range for stabilized and unstabilized raw earth, respectively 1.8 to 8.25 MPa and 0.6 to 2.25 MPa. Then, the challenge is to optimize the amount of cement in the material in an attempt to minimize the non-ecological and expensive component in the raw-earth material [4].

However, shrinkage in these raw earth-based materials is one of their weaknesses. It is responsible for the development of cracks. To reduce this effect, their plastic behavior needs to be improved to prevent brittle failures and thus limit cracking [10].

The plastic behavior of raw earth-based materials shows a ductile behavior characterized by a compressive strength that increases until it reaches a maximum value and then decreases slowly with deformation. Ductility can be parameterized to characterize the plastic behavior of the materials. Ductility is the ability of the material to deform itself without breaking. For example,

50 it is required for the various building materials in the areas of seismic risks ([11], [12]). The
51 good ductility of the material will prevent the sudden collapse of the structure. Either the
52 material is suitably ductile enough or a constituent, such as biopolymers, plant and animal
53 aggregates or fibers, is added.
54 When focusing on the plasticity of earth material, it can be noticed that the number of studies
55 is limited. Some of the studies pay attention to the determination of fiber properties since they
56 directly impact the plasticity of the composite material. The mechanical characteristics of
57 natural fibers seem to depend on cellulose content [13] and more generally on the environmental
58 conditions of plant growth or on the choice of maturity level ([14], [15]). Moreover, it can be
59 noticed that measuring techniques can partly explain the variability of measured properties (
60 [16], [17]). Vegetal fibers are natural, biodegradable and economical materials. Their addition
61 to materials has several objectives. Their main role is to reduce plastic shrinkage at early age
62 limiting the crack formation occurring during drying. Indeed, fibers allow distribution and
63 dissipation of the tensile stresses due to shrinkage of the clay fraction of the material more
64 effectively ([18], [19]). Vegetal fibers also favor the drying process by draining moisture
65 outwards through the fiber channels and contribute to lighten the building material. However,
66 Segetin et al., [20] showed that the addition of vegetal fibers may also promote shrinkage.
67 Fiber quality, quantity, and its distribution in the material directly affects the benefits and
68 disadvantages on the natural composite material. Therefore, the addition of fibers should be
69 made with care [20].
70 Some experimental studies are limited to the observation of the ductile behavior of raw earth
71 materials. For example Segetin et al., [21] in a laboratory study through the flexural test, used
72 the fiber from the New Zealand flax plant to reinforce soil-cement building materials in an
73 attempt to improve the ductility. They found that adding of 0.6% of fibers content to a soil-
74 cement matrix can significantly enhance the material ductility and avoid the failure pattern

displayed by specimens without fiber-reinforcement. Marandi et al., [22] studied the strength and ductility behavior of silty-sand soils reinforced by randomly distributed palm fibers. The composite soils were tested under laboratory conditions and examined for unconfined compressive strength. Their results showed that an increase in the fiber inclusion rate, from 0.25 % to 2.5 %, resulted in the soil being more soft and ductile. This behavior led to the failure of the soil specimens at higher axial strains. Krishna Rao et al., [23] investigated the performance of silty-sand soils reinforced with linen fiber using the unconfined compressive test. They pointed out that adding 0.75% of linen fibers has the dual benefit of increasing the stiffness and ductility of the reinforced soil. However, again, the ductile behavior was observed when comparing stress-strain curves for materials with and without fibers but the ductility property was not estimated [23].

Because of the difficulty for accurate measurement of the ductility property for porous media, few studies are effectively dedicated to estimate the ductility property of raw earth materials. In the work of Fratini et al. [24], the study of the mineralogical, physical and mechanical characterization of the adobe samples, coming from seven different old buildings in a poor state of conservation, has been carried out together with an analysis of the "local earth" for comparison. Ductility property was quantified by two parameters: the kinematic ductility and the available kinematic ductility. Both ductility parameters for the samples obtained from kneading the earth of the old bricks and the new bricks indicate a "ductile behavior" of all the bricks, with both a fairly good source of resistance after the end of the elastic behavior and a good reserve of resistance after the peak of strength. They concluded that these new bricks can be used for the restoration of the given old buildings. Park [25] performed a series of unconfined compressive tests on specimens of fiber-reinforced cemented sand. He evaluated how the fiber ratio and the cement ratio could influence the measured strength and ductility characteristics of cemented sand. The ductile behavior was quantified by the deformability index, D, which is

defined as a ratio of the axial strain at peak strength of fiber-reinforced specimen to that of non-fiber-reinforced specimen. In the case of 1% fiber ratio, the values of D were greater than 4 regardless of cement ratios. Triaxal testing was used by Consoli et al., [26] to study experimentally the influence of fiber and cement addition on the behavior of sandy soils. Their findings showed that the inclusion of 3% of fiber on the soil samples containing 1% of cement, reduced from 2.6 to 0.6 the brittleness index I_B. This index is defined as $I_B = (q_f - q_u)/q_u$, where q_f and q_u are respectively the failure and ultimate deviatoric stresses. It demonstrates that the failure behavior becomes increasingly ductile for the fibrous material.

Furthermore, numerous experimental studies were carried out to quantify ductility property of reinforced concrete ([27], [28], [29], [30], [31]). Even if reinforced concrete cannot be compared to the raw earth material, the ductility indicators defined for reinforced concrete can be used for earth material.

For complex mixtures with several components, the Design Of Experiments (DOE) approach is particularly adapted ([4], [32]). This investigating tool can be used for studying and optimizing the mechanical properties of building materials. It is no longer a question to vary successively the different components of the mixture, and the tests are defined by mathematical criteria to match with the constrained experimental domain [33]. The quality of the experimental design is based on a statistical analysis. Then characterizing and quantifying the influence of each of the components and their interactions on the considered property can be performed.

The main objective of this research paper is to quantify the ductility of a raw earth material called Cématerre, with the aim of improving its plastic behavior. Cématerre is a French company settled in Normandy region which developed a new concrete based on raw earth material, in collaboration with the University of Le Havre Normandie. Its originality is its ability to be cast in place such as a traditional concrete ([4], [19]). The choice of using flax

fibers is motivated by the important production of flax in Normandy, which is the first flax producer region in France with 55% of total production [34]. Indeed, due to the benefits outlined above, in addition to good mechanical properties, these fibers are considered as a good alternative for construction and building materials.

To fulfill this objective, combinations of five-constituent mixtures composed of flax fibers, lime, cement, water and silt were formulated by a D-optimal mixture design to investigate the ductility. D-optimal mixture design is a computer-generated design. It is a class of Design Of Experiments (DOE) which proposes the best set of experiments to be conducted via an optimization process. The optimization is based on the maximization of the determinant of the information matrix [33]. Two ductility indices were evaluated: First, the ductility index used in the literature based on the pre-peak and post-peak regions of the stress-strain curve [35] and the second, a new one estimated in the post-peak region of the stress-strain curve. The definition of these two indices is given in section 2.2.3. The experimental domain was defined according to three constraints that are presented in section 3.1: (i) the fundamental mixing constraint, (ii) an economical and ecological constraint and (iii) a workability constraint.

A series of laboratory tests was carried out to study ductility after 90 days of curing time; then the derived model was validated. The effect of each mixture component on the ductility of raw earth concrete was then analyzed through a response trace plot. Thereafter, a normalized representation of stress-strain curve was proposed to study post-peak ductility regardless of material strength.

2. Materials and experimental methods

2.1. Materials

The raw earth concrete is a mixture of several materials as described in the following section.

2.1.1. Soil material

The used building material is natural silt, chosen because it is locally available in abundance. In respect to particle size, the analysis is performed with two different methods (sieving [36], [37]) and sedimentation [38].) based on the particle diameters (Fig. 1). It should be noted that no fine-grained clay material (< 2µm) was detected as shown in the grading size distribution curve (Fig.1). For this soil, the effective diameter, the Hazen uniformity factor and the curvature factor are respectively 32 µm, 4.37 and 0.94. The Atterberg limits are respectively 20% for the liquid limit and 6% for the plasticity index. Based on Atterberg limits and grading size curve, and also according to LPC-USCS (ASTM D2487-11) standard [39], this soil is classified as silty sand (SM). Imanzadeh et al., [4] have already described the property of this silty sand in details.

2.1.2. Binders

Two binders are used to prepare a raw earth concrete: lime and cement. The used lime comes from the Proviacal® DD range. It is a calcic quicklime CL 90-Q (R5, P3), containing 90.9 % available CaO and reactivity t_{60} = 3.3 minutes [40]. The used cement is CEM I 52.5 N, in respect to the NF EN197-1 [41], NF P15-318 [42] and NF EN196-10 [43] standards. More information about these binders' properties is given in details in Eid 2017 [18].

2.1.3. Flax fibers

The used flax fibers are extracted locally from the region of Normandy. The choice of flax fibers is motivated by the important production of flax in Normandy, which is the first flax producer in France with 55% of total production [34]. Their physical and mechanical properties (density ρ, fiber diameter d, Young's modulus E, failure stress s_u and failure strain ε_u) are listed in Table 1. It is clear that these properties can vary greatly depending on the environmental conditions of plant growth, choice of maturity level and the measurement methods ([16], [17], [44]). These

mean data show that, in the domain of natural vegetal fibers, flax fibers (Fig. 2) offer good mechanical performances ranking them just after hemp fibers in terms of elastic modulus and tensile strength ([45], [46]). This is due mainly to the high cellulose and low lignin mass contents in flax fibers. Furthermore, there is a link between the cellulose content and the mechanical characteristics of fibers [13].

The used fibers are natural fibers which have not undergone any chemical surface treatment. Fibers have diameters ranging between 10 to 15 μm [47] with 50 to 70 mm lengths. According to their high aspect ratio (length/diameter), of order 5000, flax fibers ensure a good contact surface with the matrix allowing the load transfer to the material. However, their amount in specimen should be limited for different reasons. First, an excess of fibers may result in slipping phenomena between fibers and limiting friction with the mineral matrix. Furthermore, it should be noted that incorporating fibers without favoring any fiber orientation and with a final homogeneous distribution in the material is a hard task. It will be even more difficult when preparing the material as a traditional concrete on the construction site. It gives another argument in favor of a fiber content limitation. Given all these arguments, fiber content was varied in the range of 0.3% to 0.45% in mass: 0.3% was considered as a low level and 0.45% as a high level of fiber content in specimens.

2.1.4. Incorporation of a superplasticizer additive

Since raw earth concrete shrinkage depends on the amount of mixing water, the minimization of shrinkage therefore requires a limited water content. However, to preserve the consistency when manufacturing the concrete, the addition of a superplasticizer additive can be an alternative. The additive, referenced SIKA VISCOCRETE TEMPO-10, is a new generation superplasticizer based on acrylic copolymer, according to NF EN 934-2 standard [48]. It contains no chlorides or other substances likely to cause or promote the corrosion of steel, and therefore it can be used without restriction for the construction of reinforced and pre-stressed

concrete structures. The super-plasticizer contributes to deflocculating fine grains and to lubrification of the solid surfaces, decreasing the friction stresses between particles ([49], [50]). An amount of 0.3% to 0.5% of cement weight is recommended. It reduces the water content from 15% to 25% in the cement pastes without modifying the consistency. A similar dosing, based on the proportion of cement in the mixings, was chosen for present tests. A constant amount of additive of 5 ml/ m^3 has been used for each sample preparation.

A potable tap water from the pipe in the laboratory has been used for preparing the raw earth concrete.

2.2. Experimental methods

2.2.1. Sample preparation

The preparation of specimens including fibers and cement requires a particular attention to obtain homogeneous samples with a random distribution of the fibers. The mixing procedure is carried out in a laboratory mixer with a capacity of 4 liters including of two successive phases: in the first phase, a dry mixing during two minutes of soil, binders and fibers, then, in the second phase, water and additive are added for a wet mixing during three minutes. The used silt was first oven-dried at 60 °C for 48 hours in order to control the amount of water in the specimens. Thereafter, the molds of 100 mm of height and 50 mm of diameter are filled by vibration for two minutes with a vibrating table. Then, the specimens were stored in a mold for 90 days of curing-time in controlled laboratory environment (relative humidity RH ≈ 50 % and temperature: T ≈ 22 °C) prior to their testing. After 90 days of curing-time, it can be considered that the majority of the chemical reactions were achieved due to binders.

2.2.2. Unconfined Compressive Strength (UCS) test

Laboratory-prepared raw earth concrete specimens with different mix proportion were submitted to an axial Unconfined Compressive Strength (UCS) test according to NF P94-420 [51], NF P94-425 [52] French standards. The Unconfined Compressive Strength test was

229 preferred to the bending test ([28], [31], [35], [53]) because the studied raw earth concrete is
230 destined to build non-reinforced structural elements only subjected to axial compression ([25],
231 [54], [55], [56]). Therefore, the ductility parameters are estimated from the applied axial stress
232 versus axial strain curve deduced from UCS test.
233 The experimental device includes a press with a maximum load capacity equal to 100 kN and
234 a potentiometric displacement sensor with an accuracy of ± 0.05 mm connected to an
235 acquisition center which is controlled by a computer. The tests have been performed at
236 controlled displacements. A strain rate of 0.1 mm / min was chosen for all the tests. More
237 information about the experimental device was given by Imanzadeh et al. [4].
238 The unconfined compressive strength test is used to plot the material stress-strain curve. Fig.
239 3a presents the stress-strain curve for formulation F9 after 90 days of curing time. This curve
240 is used to illustrate the response curve of the studied raw earth material stabilized with binders
241 and fibers. The stress-strain curve is complex and characteristic of a ductile material with four
242 zones delineating a distinct behavior of the porous material. For low strains (A-zone), the curve
243 is concave, typical of soft porous materials. This is due both to the experiment with the
244 implementation of a homogeneous contact between the specimen and the press and to a physical
245 process: the closure of natural microcracks in the porous material stabilized with binders. As
246 strain increases more, the material already undergoes large deformation. The linear curve
247 portion with maximum slope is detected (B-Zone). At the beginning of C zone, the stress-strain
248 curve exhibits significant nonlinearity. The C zone is described as a plastic zone, usually
249 associated to the non-linear phase due to micro-cracking. The material gains its strength thanks
250 to the strong bonds developed from cementation and internal friction. The slope decreases due
251 to breaking of the cement bonds until the maximum compressive strength is reached. At this
252 point, all the cement bonds at the failure surface have broken. The post-peak zone (D-zone)
253 corresponds to the material behavior after the appearance of a failure plane. The observed

reversal of the stress-strain curve is the consequence of the ductile nature of the raw earth material. Flax fibers tend to maintain a relative cohesion of the material that exhibit a ductile failure.

2.2.3. Tools for ductility analysis

To study the ductility of the material, two ductility indices *i* and *i'* are proposed and used to characterize the ability of the material to withstand plastic deformation. The first one is representative for the major part of the plastic zone ([35], [57]) and the second one focuses on the post-peak behavior. The *i* index is an adapted form of the displacement ductility index defined by Cohn and Bartlett [27] for cement concrete. The *i* index is defined as $i = \varepsilon_3/\varepsilon_1$ (Eq. 1) where ε_3 refers to the axial strain when UCS drops down to 0.85 times of UCS_{max} and ε_1 refers to the axial strain when the tangent to the linear section of maximum slope intercepts UCS_{max} line (Fig. 3b).

$$i = \frac{\varepsilon_3}{\varepsilon_1} \qquad Eq.1$$

The *i*' ductility index is defined as $i' = \varepsilon_3/\varepsilon_2$ (Eq. 2) where ε_2 refers to the axial strain for UCS_{max} (Fig. 3b).

$$i' = \frac{\varepsilon_3}{\varepsilon_2} \qquad Eq.2$$

3. Experimental design

The considered mixture constraints are described in the following section before explaining the generation of the experimental design.

3.1. Mixture constraints

Three constraints must be considered:

- Fundamental constraint where the sum of the ingredients of the mixture is 100 % in weight for all the mixes of the design: Fiber % + Lime % + Cement % + Water % + Silt % = 100 %

- Economical and ecological mixture constraints: The raw earth concrete has to be designed to provide the appropriate mechanical and durability properties to be used as a construction building material. In addition, it should be non-energy-intensive in regard to gray energy. Thus, the percentage of added binders (cement and lime) should be limited. For these reasons, the maximum quantities of cement and lime are respectively limited to 16% and 12% [4]. Then, the following condition must be verified: Cement % + Lime % < 16 %.

In agreement with the mentioned constraints above, mixing range chosen for each of the constituents, using fiber, is presented in Table 2.

- Workability constraint: workability plays an important role on the mechanical properties. It depends on several properties such as consistency, plasticity and cohesion ([58], [59]). Consistency is, unlike plasticity and cohesion, easy to measure. That is why it is currently used to characterize workability. The classes of consistency were measured on fresh mixtures, according to Abrams cone test (standard NF EN 206-1 [60]). A S3 level of consistency calibrated by standard slump test was chosen to ensure a fluidity similar to a very plastic concrete. A preliminary experimental design [2] was conducted to evaluate a multiple linear regression equation for consistency (Eq. 3). The condition of suitable consistency level (slump S3) sets the boundaries of the equation validity. The condition fitted for mixings with fibers was compared to the equation established for raw earth materials without fibers (Eq. 4, [2], [4]) according to a similar experimental protocol.

The resolution of workability equations with the condition of fundamental constraint and economical and ecological mixture constraints delineates the regions of acceptable mixtures. The 4- or 5- dimensional spaces defined by Eq. 3 and Eq. 4 were projected in the (cement, water) plane. Fig. 4 depicts the domains of valid workability condition for the proportion of lime fixed to X_{lime} =0.02. It is representative of what occurs in the whole domain of workability condition validity. It is shown that the two regions are very close with an increase in order of

1-2% of water content for mixtures with fibers compared to mixtures without fibers. In spite of the hydrophilic nature of fibers (absorption >100% for flax fibers [14], [61]), it highlights the important water-reducer role of the plasticizer admixture used for tests with fibers.

$$2.5 \leq 1.7 - 0.3\,\text{fiber} - 19\,\text{lime} - 6\,\text{cement} + 28\,\text{water} - 7.5\,\text{silt} \leq 2.7 \quad \text{Eq. 3}$$

$$2.5 \leq -22\,\text{lime} - 9\,\text{cement} + 42\,\text{water} - 9\,\text{silt} \leq 2.7 \quad \text{Eq. 4}$$

3.2. Generation of the experimental design

In this research study, experimental region is constrained by three conditions (see section 3.1) to an irregular 3D-polyhedron. Thereafter, D-optimal design based on a computer-aided is adapted to generate the set of experiments. The selection process of the best candidate set of experiments is performed by a D-optimal criterion, applied to maximize the information contained in the different possible data sets and the quadratic model that will be fitted. The G-efficiency criterion is then estimated to choose the best D-optimal data set [62]. The efficiency values of at least 50% are considered acceptable for design purposes [63].

In this study, the mixture design was developed through a D-optimal design including three constraints (see section 3.1). A sub-set of 27 formulations was selected from the candidate set proposed by MODDE© software. This choice is validated by a good level of design statistics indicators of efficiency. Indeed, the G-efficiency measure is equal to 66.04 % [64]. The 27 formulations (Table 3) were tested in the random run order suggested by the software [65] with two repetitions. Three estimations at the center point of the experimental domain were included. The center point plays an important role. It is used to estimate the variability of the response as well as curvilinear effects. Thereafter, the Partial Least Square projections to latent structures (PLS) adapted to complex experimental design data [66] were used to calculate the model coefficients. For each formulation, three specimens were tested and the mean of the measured values was considered except for the center point for which the three data were entered (F25,

F26 and F27, Table 3). The measured values for both ductility indices *i* and *i'* are also presented in Table 3. Furthermore, the standard deviation of ductility index was calculated for the different formulations. All the standard deviations (σ) are smaller than 0.1 except for formulation F21 (σ = 0.16). Due to the small standard deviations, the ductility values can be considered with confidence.

4. Statistical analysis of regression models

Quadratic polynomial model was applied to the five-component mixings issued from the experimental design to make the prediction of the two ductility indices *i* and *i'*. This quadratic model includes the different terms in relation to the binary interactions for all possible pairs of ingredients ([67] [68]).

The Analysis Of Variance (ANOVA) includes several diagnostic tools that are used to validate models ([64], [68], [67]). The two first diagnostic tools are the regression coefficients (R^2 and R^2_{adj}), informing on the ability of the model to fit the measured data. Furthermore, Q^2 coefficient estimates the model validity *i.e.*, its ability to predict new data. The model validity should also be verified ([69], [67]).

The first F-Test is the regression model significance test. It compares regression variance (SS_R) to residual variance (SS_r). The critical Fisher value for a probability at a fixed 95% confidence interval should be smaller than estimated F-value for the model. It reflects the statistical ability of prediction of the model.

For the second F-Test (also called the lack of fit test), residual error is decomposed in two parts: lack of fit (LOF) due to imperfection of the model and Pure Error (PE) estimated from replicates data error. The calculated F-value for the model should be smaller than the critical acceptable value at 95% confidence interval.

5. Results

5.1. Observations

All the specimens failed in a ductile manner with ductility indices varying between 1.27 and 5.12 for *i* index and between 1.13 and 2 for *i'* index (Table 3). It can be noted that some data are missed in Table 3. Five formulations are concerned (F2, F4, F5, F15 and F19). These specimens show steadily increases of the strength with no maximum compressive strength reached. The example of formulation F2 is given in Fig. 5.

The classical failure with a well-identified inclined plane is observed when the smallest dimension of the sample is 10 times larger than the size of the biggest particles in the specimen which guarantees the mechanics of continuous media hypothesis [70]. For mixtures with fibers, the failure mode can differ from the classical one, as the length of fibers can be as large as the diameter of the specimen. For some formulations, the mechanics of continuous media hypothesis is no longer valid. Therefore, the failure mode becomes random and the failure plane can intersect the top and the bottom of the sample. The friction at the top and at the bottom prevents the development of the failure, and in this case, a continuous increase in strength is observed, without observing a peak of maximum strength. These observations are consistent with the results of the literature on bio-materials based on plant fibers [71].

The evaluation of ductility indices cannot be performed for these five specimens and these cases are disregarded for the ductility exploration. Thus, indices were calculated for 22 different formulations. The variation range, by a factor of 4.03 for *i* and 1.77 for *i'* is relevant of a strong dependence with the composition of mixtures (Fig. 6).

As mentioned earlier, the tests order is random and successive formulations correspond to materials with proportions of the five components while vary all together. Ductility analysis cannot be conducted from the direct analysis of Fig. 6 and an approach by DOE is presented in the next section. However, some general remarks can be made. First, it was found that for some

specimens (for example F1), *i'* index is close to unity and *i* index tends to *i'* index. A *i=i'=1* condition would correspond to brittle failure of fragile material that hardens with a constant rate and then breaks suddenly when its maximum strength is reached. It is also shown that the two indices clearly do not exhibit the same evolution with a greater amplitude of variation for *i* index than for *i'* index. Finally, four formulations (F3, F6, F16 and F17) are noticed to have much greater *i* index among the others. As the generation of mixture planification by DOE insures a good repartition of formulations in the constrained experimental domain, the four formulations mentioned above, corresponding to the most ductile specimens tested, need to be examined with attention.

5.2. Model validation

Linear and quadratic polynomial models were first fit to the measured experimental data to identify the most adequate models representing the measured experimental data. The coefficients of the linear and quadratic models for *i and i'* ductility indices were given in Table 4. The values of R^2, R^2_{adj} and Q^2 were presented in Table 5. As shown in Table 5, for *i'* ductility index, the two regression coefficients (R^2, Q^2) noticeably increase when a quadratic model is chosen. Indeed, the interactions between components of the mixture are strong, pointed out by large values of interaction coefficients (Table 4). This indicates a non-linear dependence of the ductility property with the mixture components. However, one can also note a slight decrease in the R^2_{adj} coefficient. Otherwise, for *i* ductility index, all the three coefficients are smaller than the ones obtained for *i'* ductility index, for both linear and quadratic models. Furthermore, the statistic indicators of the model validity for *i* are very low. It can be concluded that a quadratic model can be adapted for *i'* ductility index but it failed for *i* ductility index. Then, the statistical model validation procedure for *i'* ductility index is continued via F-tests of ANOVA.

Concerning the first F-Test for *i'*, the model F-values are higher than the critical Fisher values for a probability at a 95% confidence level (Tables 6 and 7). The P-value is smaller than the

significance level, which shows that that selected model passed the first F-Test. For the second F-Test, the residual error and the pure error from replication are compared and F-values for the model are estimated. In respect to the criterion, the estimated F-value for the model is significantly smaller than the critical acceptable value at 95% confidence interval with an acceptable P value equal to 0.56 (Tables 6 and 8). Thus, one can reasonably consider that chosen model is valid. Once the best-fit model was selected, an equation for the post-peak ductility index *i*' was provided for the studied raw earth concrete.

One can conclude at the end of this section that it is possible to modelize the ductile behavior of raw earth material stabilized with lime, cement and fibers in the post-peak zone. In the D-zone of stress-strain curve, material undergoes deformation without breaking, tending towards a residual strength, because of internal friction that is the only mechanism that sustains the material. The difficulty to determine a reliable model for *i* index indicates that characterizing all the plastic domain for this five-component material is a hard task. The pre-peak zone where material exhibits an elasto-plastic behavior cannot be predicted accurately. Indeed, the debonding of the cementitious matrix and friction between the matrix and fibers are mechanisms that contribute in a complex imbricated manner to ductility.

5.3. Response trace plot of post-peak ductility index

The response trace plot is a useful tool to observe the behavior of the predicted values versus the change of proportion of each constituent. Response trace plots were performed; the response of ductility index *i'* was drawn around a reference mixture. In this research study, the considered reference mixture is the centroid of the constrained experimental domain with the quantities of fiber, lime, cement, water and silt respectively equal to 0.375 %, 3.015 %, 8.402 %, 23.953 % and 64.255 %.

Response trace plots of ductility index *i'* with deviation from reference mixture in proportion for 90 days of curing time, for the quadratic and linear models, were shown in Fig. 7. This figure

points out how each constituent influences on predicted ductility index in respect to the reference mixture. For the reference mixture, the ductility index value is equal to 1.53 (Fig. 7). The ductility index values are very sensitive to changes in cement and silt proportions. The steep slope for silt shows the major influence of this constituent. Figure 7 indicates that an increase of silt proportion in the mixing tends to increase the ductility index. Indeed, since silt exhibits an elasto-plastic behavior and is naturally ductile, it can withstand large strains during loading. Therefore, an increase of silt proportion in the mixture promotes the plasticity of the material, therefore its ductility.

Concerning the cement influence, an increase of the proportion of cement in the mixing decreases the ductility index. This negative effect on ductility is due to pozzolanic chemical reactions involving cement that generate a very hard bond between the soil particles. When the load reaches its maximum strength, and even when the cement proportion increases, links can break suddenly in a brittle way.

Water and water interaction effect with the other constituents (quadratic model) show a negative effect on the ductility index (Fig. 7 a). In contrast, Fig. 7b shows the positive effect of water in the absence of the water interaction effect with other constituents (linear model). The latter model points out that this negative effect in the quadratic model is due to the water interaction effect with binders. Indeed, when the amount of water increases, the excess water, that is not necessary for the hydration of the binders, evaporates. This evaporation generates a suction (negative pore water pressure) which is at the origin of the shrinkage of soils. This shrinkage induces a densification of the material and consequently decreases its ductility.

The response trace for lime has a negative slope indicating a decrease on the ductility index. Since lime is a binder, its effect is similar to that of cement as explained above.

Concerning the fiber effect, the steep slope for fiber indicates the major influence of this component compared with other components. However, its positive effect on the ductility index

459 is very limited because of the small range of variation of fiber proportion in mixings between
460 0.3% and 0.45%. To study the influence of fiber content, it is required to increase the range of
461 its variation.

462

463 **6. Discussion**

464 As mentioned in the introduction, ductility is a desired property but apparently not quantified
465 for raw-earth material. Discussion focuses on a further analysis of the evolution of the two
466 ductility indices concerning fiber content influence and (silt/binders) ratio that emerge as a
467 relevant parameter.

468 6.1. *Normalized representation of stress-strain curve*

469 In order to compare more easily the ductility level of the specimens, a normalized representation
470 of the stress-strain curve is used (Fig. 8). The y-axis designates UCS* defined as UCS/UCS_{max}
471 where UCS_{max} stands for the maximum compressive stress and the *x*-axis designates $\varepsilon^*=\varepsilon/\varepsilon_{max}$
472 where ε_{max} is the strain associated to UCS_{max}. This representation is particularly adapted to
473 compare ductility of different materials since curves are gathered together at the same scale for
474 the two axes. The stress-strain curves for the two formulations F1 and F22 are plotted in a
475 normalized form (Fig. 8). With this plot, ductility can be characterized regardless of the
476 maximum stress level of the material. The arrow directly gives the *i'* post-peak ductility index
477 because the strain associated to UCS_{max} is equal to unity for all materials. The length of the pre-
478 peak and post-peak zones can also be compared. A marked dissymmetry of the plastic domain
479 is noted for the two specimens with a greater extension of the post-peak zone compared to the
480 pre-peak zone. Of course, the two domains are more extended for the more ductile material
481 (F22) containing fewer binder. A steeper slope of the linear zone is noted for the more ductile
482 material. It should be noted that the slope does not reflect the strain modulus of the material in
483 this normalized representation.

484

485 6.2. *Influence of fibers*

486 The normalized stress-strain curves are represented for pairs of formulations almost similar
487 except by the fiber content that can be low (fibers = 0.3%) or high (fibers = 0.45%). This
488 normalized representation is a useful tool to evaluate *i'* ductility index, as its value can be
489 directly read on the x-axis. Three different comparisons are plotted on figure 9 a, b and c
490 respectively for (F7, F8), (F20, F9) and (F3, F6). While when the ductility is low (Fig. 9a), a
491 weak influence of the variation of fiber content is noted, a clear difference is shown for the
492 more ductile materials (Fig. 9 b and c). The material containing 0.45% fibers is more ductile
493 than the one containing 0.3%. From Fig. 9, one can deduce the ductility index *i'* and $\varepsilon^* = \varepsilon_1/\varepsilon_{max}$
494 as shown in Table 9. For example, in Fig. 9 b, *i'* is about 1.29 for 0.35% of fibers and *i'* is 1.41
495 for 0.45%. It also seems that pre-peak zone is more affected by the level of fiber content than
496 post-peak zone. As shown in this table, for example for Fig. 9 b, the value of ε^* is equal to 0.82
497 for the fibers content of 0.35% and 0.69 for the fibers content of 0.45%.

498
499

500 6.3. *Influence of (silt/binder) ratio on ductility indices*

501 In the experimental domain studied, the range of (silt/binders) ratio was defined on an extended
502 range from 3.5 to 18. Ductility values for the two indices, issued from the DOE study (see
503 section 5.2, Table 4) and obtained experimentally are shown in Fig 10 as a function of
504 (silt/binders) ratio. For a ratio of 1:18 between silt and binders, binder proportion was reduced
505 to 5.6% compared to silt proportion while for 1:3.5, more than 25% of binders proportion is
506 reached. As expected, the breaking is more brittle when (silt/binders) ratio is decreased. If soil
507 particles are not completely enclosed by binders when the ratio of silt/binders increases, the
508 ductile influence of silt becomes predominant and ductility increases. On the contrary, when
509 silt/binders ratio decreases due to an increase in binder proportion, the cement chains break
510 abruptly and this leads to a decrease in ductility. Furthermore, the two indices increase when

511 the binders proportion decreases compared to silt proportion, whatever the fibers content in the
512 range tested. One can also note that *i'* index seems to saturate when a threshold ratio, around
513 13, is exceeded. This means that when the (silt/binders) ratio exceeds 13, the ductility value *i'*
514 can converge towards the ductility of the untreated silt (without binders). Since a clear
515 dependence of *i'* ductility index with (silt/binders) ratio is observed, the search for an
516 experimental law was conducted. In the range of compositions tested, the post-peak ductility
517 index *i'* can be expressed in the form of a 2nd order polynomial (Eq. 5, Fig. 10) with a regression
518 coefficient of R^2= 0.94. However, the use of such a law needs to be very careful because of the
519 great dependence on the experimental protocol chosen for the preparation of test specimens.
520
521 $i' = -0.004\,(\text{silt} / \text{binders})^2 + 0.14\,(\text{silt} / \text{binders}) + 0.79$ with R^2=0.94 Eq. 5
522
523 All the formulations were used to find a relation between *i'* and the silt/binder ratio. The
524 independence of *i'* with the fiber proportion in Eq. 5 does not mean that fiber does not affect
525 ductility but that no significant change in ductility is noted when the fiber proportion varies in
526 the testing range (0.3% to 0.45%).
527 As was already noted when results of DOE were analyzed (see section 5.2), it was not possible
528 to propose a similar model for *i* index. Indeed, as mentioned above, the four formulations F3,
529 F6, F16 and F17 are characterized by very high *i* values compared to the other formulations.
530 The observed gap in *i* index can be supported by the idea that - for formulations with low binder
531 proportion with respect to silt - chains of cementitious bonds between silt particles are short
532 and do not allow the development of a rigid matrix. Thus, during the loading phase, chains
533 simultaneously and brutally break, independently of the silt/binders ratio as long as this ratio is
534 large enough (silt/binders >7-8). Then, only the ductile influence of silt and fibers remains.

The ductility of the studied materials described by the *i* index adapted from the literature is at most 3 times the ductility of a brittle material. Raw earth reinforced with flax fibers could then reach a ductile level, providing an interesting damage tolerance.

The ductility index *i'* reflects only partially the plastic nature of the material. However, if a level of strength is achieved for a material, the knowledge of the post-peak ductility may be sufficient to conclude on its ability to deform. Actually, a high *i'* indicator is always associated to a high *i* indicator. Furthermore, a factor of about 2 for the range of variation of *i'* index is convenient to evaluate significant changes in the material behavior in the post-peak region of the stress-strain curve.

The comparison between present ductility indices (*i* and *i'*) with those from the literature is limited. Indeed, the ductile behavior is generally observed on stress-strain curve in axial loading test or force-displacement curve in bending test but ductility index is rarely estimated and analyzed. Present data for *i* ductility index were compared to data on reinforced cement concrete from Rakhshanimehr et al., [35]. A similar range of *i* index is found for the two types of materials: 1.15 to 7 for reinforced cement concrete [35] and 1.27 to 5.12 for the studied raw earth concrete. No data is available in the literature for *i'* index introduced herein.

Finally, the discussion confirms that the relevant parameter for quantifying ductility is the ductility index *i'* since it is adapted to the study of all the stress-strain behaviors in the range of material tested.

7. Conclusion

A building eco-material based on raw earth stabilized with binders and vegetal fibers was produced. The ductile behavior is one of the desired characteristics particularly in the context of an exploitation in seismic zones and the quantification of this mechanical property is necessary. Among the constraints associated to the sample preparation of materials with varying

560 cement and fiber content, the workability condition is essential. The major role of the super-
561 plasticizer admixture is pointed out for the elaboration of workable material with fibers.
562 The axial stress-strain curve provides the basis to study ductility. An alternative ductility index
563 was proposed in order to evaluate post-peak behavior of ductile raw earth material stabilized
564 with fibers. It can be easily evaluated on the basis of a normalized representation of the stress-
565 strain curve of the material. By using this new tool, post-peak ductility of different materials
566 can be directly compared regardless of their compressive stress. Ductility of present specimens
567 was studied with a mixing design. The post-peak plastic domain described by the *i'* ductility
568 index, where fibers play a key role was studied and modelized successfully with a quadratic
569 model. Strong interactions between the components of the mixing are demonstrated. In contrast,
570 ductility of the plastic domain defined by *i* ductility index, could not be modelized. It indicates
571 the difficulty to predict ductility of this domain dominated by brittle cement bonds breakings
572 and mobilized friction processes. In an attempt to understand the influence of mixing
573 composition on ductility, silt/binders ratio was calculated and its influence on ductility index
574 was clearly pointed out. The ability of fibers to reinforce ductility property increases with
575 silt/binders ratio. An increase in the mobilized friction can be linked the silt-fiber interface
576 increases. Consequently, the collapse of the material is delayed and the ductility is increased.
577 In the light of its ability to predict post-peak ductility of a raw earth material with fibers, the
578 use of *i'* alternative ductility index could be extended to other raw earth materials. Finally, *i'*
579 index could be used to define a ductility criterion to meet specific requirements of seismic
580 regions.
581 The difference in content over the range of testing fibers (0.3 to 0.45% in mass) does not impact
582 significantly the ductility performance of the earthen material. Further investigation with a
583 larger range of fiber content should be undertaken to analyze its influence and to optimize its
584 content.

Acknowledgement

The authors wish to express their gratitude to the company Cématerre, the CNRS (French National Center for Scientific Research) and the FEDER (European Economic and Social Development Fund) for their support.

591 **References**
592

[1] P. Přikryl, Á. Török, M. Theodoridou, M. Gómez-Heras and K. Miskovsky, "Geomaterials in construction and their sustainability, Sustain. Use Tradit," *Geomaterials Constr. Pract.,* p. 1–22, 2016, doi: 10.1144/SP416.21.

[2] A. Hibouche, Sols traités aux liants, Performances hydro-mécaniques et hygro-thermiques, Applications en BTP, Dissertation, Normandie Univ., UNIHAVRE, 2013.

[3] P. Zak, T. Ashour, A. Korjenic, S. Korjenic and W. Wu, "The influence of natural reinforcement fibers, gypsum and cement on compressive strength of earth bricks materials," *Constr. Build. Mater.,* vol. 106, p. 179–188, 2016, doi: 10.1016/j.conbuildmat.2015.12.031.

[4] S. Imanzadeh, A. Hibouche, A. Jarno and S. Taibi, "Formulating and optimizing the compressive strength of a raw earth concrete by mixture design," *Constr. Build. Mater.,* vol. 163, p. 149–159, 2018, doi:10.1016/j.conbuildmat.2017.12.088.

[5] T. Ashour, A. Korjenic, S. Korjenic and W. Wu, "Thermal conductivity of unfired earth bricks reinforced by agricultural wastes with cement and gypsum," *Energy Build.,* vol. 104, p. 139–146, 2015, doi:10.1016/j.enbuild.2015.07.016.

[6] J. M. Kanema, J. Eid and S. Taibi, "Shrinkage of earth concrete amended with recycled aggregates and superplasticizer: Impact on mechanical properties and cracks," *Mater. Des.,* vol. 109, p. 378–389, 2016, doi:10.1016/j.matdes.2016.07.025.

[7] M. Al-Mukhtar, A. Lasledj and J. F. Alcover, "Lime consumption of different clayey soils," *Appl. Clay Sci.,* vol. 95, p. 133–145, 2014, doi:10.1016/j.clay.2014.03.024.

[8] A. Lasledj, Traitement des sols argileux à la chaux : processus physico-chimique et propriétés géotechniques, PhD Thesis. University of Orleans, France, 2009, p. 361.

[9] M. Carmen Jimenez Delgado and I. Canas Guerrero, "Earth building in Spain," *Constr. Build. Mater. ,* vol. 20, p. 679–690, 2006, doi:10.1016/j.conbuildmat.2005.02.006.

[10] E. Araldi, E. Vincens, A. Fabbri and J. P. Plassiard, "Identification of the mechanical behavior of rammed earth including water content influence," *Mater. Struct.,* pp. 51-88, 2018, doi:10.1617/s11527-018-1203-2.

[11] F. Loccarini, Behaviour of rammed earth structures: Sustainable materials and strengthening techniques, PhD dissertation, Civil Engineering and Environmental Sciences, University of Braunschweig – Institute of Technology and Department of Civil and Environmental Engineering, University of Florence, Italy, 2017.

[12] P. H. Joen and R. Park, "Flexural strength and ductility analysis of spirally reinforced prestressed concrete piles," *PCI JOURNAL,* pp. 64-83, 1990.

[13] Y. Millogo, J. C. Morel, J. E. Aubert and K. Ghavami, "Experimental analysis of Pressed Adobe Blocks reinforced with Hibiscus cannabinus fibers," *Constr. Build. Mater.,* vol. 52, p. 71–78, 2014, doi:10.1016/j.conbuildmat.2013.10.094.

[14] K. Charlet, Contribution à l'étude de composites unidirectionnels renforcés par des fibres de lin : relation entre la microstructure de la fibre et ses propriétés mécaniques, Dissertation, Université de Caen, 2015.

[15] S. H. Hulleman, J. M. Van Hazendonk and J. E. Van Dam, "Determination of crystallinity in native cellulose from higher plants with diffuse reflectance Fourier transform infrared spectroscopy," *Carbohydrate Research,* vol. 261, p. 163–172, 1994.

[16] S. M. Hejazi, M. Sheikhzadeh, S. M. Abtahi and A. Zadhoush, "A simple review of soil reinforcement by using natural and synthetic fibers," *Constr. Build. Mater.,* vol. 30 , p. 100–116, 2012, doi:10.1016/j.conbuildmat.2011.11.045.

[17] H. L. Bos, M. J. Van den Oever and O. C. Peters, "Tensile and compressive properties of flax fibres for natural fibre reinforced composites," *Journal of Materials Science,* vol. 37, no. 8, pp. 1683-1692, 2002.

[18] J. Eid, "New construction material based on raw earth: cracking mechanisms, corrosion phenomena and physico-chemical interactions," *Eur. J. Environ. Civ. Eng.,* vol. 8189, p. 1–16, 2017, doi:10.1080/19648189.2017.1373707.

[19] J. Eid, S. Taibi, J. M. Fleureau and M. Hattab, "Drying, cracks and shrinkage evolution of a natural silt intended for a new earth building material. Impact of reinforcement," *Constr. Build. Mater.,* vol. 86, p. 120–132, 2015, doi:10.1016/j.conbuildmat.2015.03.115.

[20] H. Khelifi, T. Lecompte, A. Perrot and G. Ausias, "Mechanical enhancement of cement-stabilized soil by flax fibre reinforcement and extrusion processing," *Mater. Struct. Constr.,* vol. 49, p. 1143–1156, 2016, doi:10.1617/s11527-015-0564-z.

[21] M. Segetin, K. Jayaraman and X. Xu, "Harakeke reinforcement of soil-cement building materials: Manufacturability and properties," *Build. Environ.,* vol. 42, p. 3066–3079, 2007, doi:10.1016/j.buildenv.2006.07.033.

[22] S. M. Marandi, M. H. Bagheripour, R. Rahgozar and H. Zare , "Strength and Ductility of Randomly Distributed Palm Fibers Reinforced Silty-Sand Soils," *Am. J. Applied Sci.,* vol. 5, no. 3, p. 209–220, 2008,.

[23] S. V. Krishna Rao and A. M. Nasr, "Laboratory study on the relative performance of silty-sand soils reinforced with linen fiber," *Geotech. Geol. Eng.,* vol. 30, p. 63–74, 2012, doi:10.1007/s10706-011-9449-2.

[24] F. Fratini, E. Pecchioni, L. Rovero and U. Tonietti, "The earth in the architecture of the historical centre of Lamezia Terme (Italy): Characterization for restoration," *Applied Clay Science,* vol. 53, p. 509–516, 2011, doi:10.1016/j.clay.2010.11.007.

[25] S. S. Park, "Unconfined compressive strength and ductility of fiber-reinforced cemented sand," *Constr. Build. Mater.,* vol. 25, p. 1134–1138, 2011, doi:10.1016/j.conbuildmat.2010.07.017.

[26] N. C. Consoli, P. D. Prietto and L. A. Ulbrich, "Influence of fiber and cement addition on behavior of sandy soil," *J. Geotech. Geoenvironmental Eng.,* vol. 124, p. 1211–1214, 1998.

[27] M. Z. Cohn and M. Bartlett, "Computer-simulated flexural tests of partially pre-stressed concrete sections," *ASCE Journal of Structural Division,* vol. 108(ST12), p. 2747–2765, 1982, .

[28] A. Azizinamini, R. Pavel, E. Hatfield and S. K. Gosh, "Behavior of lap-spliced reinforcing bars embedded in high strength concrete," *ACI Structural Journal,* vol. 96, no. 5, p. 826–836, 1999, doi:10.14359/737 .

[29] M. R. Esfahani and M. R. Kianoush, "Development/splice length of reinforcing bars," *ACI Structural Journal,* vol. 102, no. 1, p. 22–30, 2005, doi:10.14359/13527.

[30] A. Perrot, D. Rangeard, F. Menasria and S. Guihéneuf, "Strategies for optimizing the mechanical strengths of raw earth-based mortars," *Constr. Build. Mater.,* vol. 167, p. 496–504, 2018, doi:10.1016/j.conbuildmat.2018.02.055.

[31] J. Claramunt, H. Ventura, L. Fernández-Carrasco and M. Ardanuy, "Tensile and flexural properties of cement composites reinforced with flax nonwoven fabrics," *Materials,* vol. 10, no. 2, p. 215, 2017, 215. doi:10.3390/ma10020215.

[32] R. H. Myers, D. C. Montgomery and C. M. Anderson-Cook, Response surface methodology: process and product optimization using designed experiments, 4th ed., New York: Wiley, 2016, p. 856 .

[33] L. Eriksson, E. Johansson, N. Kettaneh-Wold, C. Wikström and S. Wold, Design of Experiments: Principles and Applications, Learnways AB, Ume˚a, 2000, pp. 425, ISBN 91-973730-4-4.

[34] B. Abbar, A. Alem, S. Marcotte, A. Pantet, N. D. Ahfir, L. Bizet and D. Duriatti, "Experimental investigation on removal of heavy metals (Cu 2+ , Pb 2+ , and Zn 2+) from aqueous solution by flax fibres," *Process Safety and Environmental Protection,* vol. 109, p. 639–647, 2017, http://dx.doi.org/10.1016/j.psep.2017.05.012.

[35] M. Rakhshanimehr, M. R. Esfahani, M. R. Kianoush, B. A. Mohammadzadeh and S. R. Mousavi, "Flexural ductility of reinforced concrete beams with lap-spliced bars," *Can. J. Civ. Eng.,* vol. 41, p. 594–604, 2014, doi:10.1139/cjce-2013-0074.

[36] Standard AFNOR: NF P94-056, Sols: reconnaissance et essais-Analyse granulométrique-Méthode par tamisage à sec après lavage, 1996.

[37] Standard AFNOR: XP P94-041, Sols: reconnaissance et essais-Identification granulométrique-Méthode de tamisage par voie humide, 1995.

[38] Standard AFNOR: NF P94-057, Sols: reconnaissance et essais-Analyse granulométrique des sols-Méthode par sédimentation, 1992.

[39] ASTM D2487-11: Standard classification of soils for engineering purposes (Unified Soil Classification System), 2012.

[40] Standard AFNOR: NF EN 459-1, Chaux de construction - Partie 1: définitions, spécifications et critères de conformité, 2012.

[41] Standard AFNOR: NF EN197-1, Cement Part 1: composition, specifications, and conformity criteria for common cements, 2001.

[42] Standard AFNOR: NF P 15-318, liants hydrauliques ciment à faible chaleur d'hydratation initiale et à teneur en sulfures limitée, 1991.

[43] Standard AFNOR: NF EN196-10, Méthodes d'essais des ciments-Partie 10: Détermination de la teneur en chrome (VI) soluble dans l'eau des ciments, 2015.

[44] R. Girault, F. Bert, C. Rihouey, A. Jauneau, C. Morvan and M. Jarvis, "Galactans and cellulose in flax fibres : putative contributions to tensile strength," *Int J Bio Macromol,* vol. 21, pp. 179-188, 1997.

[45] A. Laborel-Préneron, J. E. Aubert, C. Magniont, C. Tribout and A. Bertron, "Plant aggregates and fibers in earth construction: A review," *Constr. Build. Mater.,* vol. 111, p. 719–734, 2016, doi:10.1016/j.conbuildmat.2016.02.119.

[46] N. H. Dhakal, Z. Y. Zhang and M. O. Richardson, "Effect of water absorption on the mechanical properties of hemp fibre reinforced unsaturated polyester composites," *Compos. Sci. Technol.,* vol. 67, p. 1674–1683, 2007, doi:10.1016/j.compscitech.2006.06.019.

[47] B. Abbar, A. Alem, A. Pantet, S. Marcotte, N. D. Ahfir and D. Duriatti, "Experimental investigation on removal of suspended particles from water using flax fibre geotextiles," *Environmental Technology, Taylor & Francis Group,* pp. 1-15, 2017, http://dx.doi.org/10.1080/09593330.2017.1284270.

[48] Standard AFNOR: NF EN 934-2, Adjuvants pour béton, mortier et coulis - Partie 2: adjuvants pour bétons. Définitions et exigences, 1998.

[49] A. Pierre, R. Mercier, A. Foissy and J. M. Lamarche, "The adsorption of cement superplasticizers on to mineral dispersions," *Adsorption Science & Technology,* vol. 6, no. 4, pp. 219-231, 1989.

[50] P. C. Aitcin, C. Jolicoeur and J. G. MacGregor, "Superplasticizers: how they work and why they occasionally don't," *Concrete International,* vol. 16, no. 5, p. 45–52, 1994.

[51] Standard AFNOR: NF P94-420, Détermination de la résistance à la compression uniaxiale, 2000.

[52] Standard AFNOR: NF P94-425, Méthodes d'essai pour roches - Détermination du module d'Young et du coefficient de Poisson, 2002.

[53] A. P. Fantilli, B. Chiaia and A. Gorino, "Fiber volume fraction and ductility index of concrete beams," *Cem. Concr. Compos.,* vol. 65, p. 139–149, 2016, doi:10.1016/j.cemconcomp.2015.10.019.

[54] M. H. Maher and Y. C. Ho, "Mechanical properties of Kaolinite/fiber soil composite," *J. Geotech. Eng.,* vol. 120, no. 8, p. 1381–93, 1994, https://doi.org/10.1061/(ASCE)0733-9410(1994)120:8(1381).

[55] A. B. Groeneveld, T. M. Ahlborn, C. K. Crane, C. A. Burchfiel and E. N. Landis, "Dynamic strength and ductility of ultra-high performance concrete with flow-induced fiber alignment,"

International Journal of Impact Engineering, vol. 111, pp. 37-45, 2017, http://dx.doi.org/10.1016/j.ijimpeng.2017.08.009.

[56] N. C. Consoli, J. P. Montardo, M. Donato and P. D. Prietto, "Effect of material properties on the behaviour of sand–cement–fibre composites," *Ground Improv,* vol. 8, no. 2, p. 77–90, 2004, https://doi.org/10.1680/grim.2004.8.2.77.

[57] C. K. Ma, A. Z. Awang and W. Omar, "Flexural ductility design of confined high-strength concrete columns: Theoretical modelling," *Measurement,* vol. 78, p. 42–48, 2016, http://dx.doi.org/10.1016/j.measurement.2015.09.039.

[58] W. C. Panarese, S. H. Kosmatka and F. A. Randall, Concrete masonry handbook for architects, engineers, builders, 5th ed ed., Skokie, Ill. : Portland Cement Association, Libraries Australia, 1991.

[59] Q. B. Bui, J. C. Morel, S. Hans and P. Walker, "Effect of moisture content on the mechanical characteristics of rammed earth," *Constr. Build. Mater.,* vol. 54, p. 163–169, 2014, doi:10.1016/j.conbuildmat.2013.12.067.

[60] Standard AFNOR: NF EN 206-1/CN, Béton–Partie 1: Spécification, performances, production et conformité (in French), 2012.

[61] S. Chafei, F. Khadraoui, M. Boutouil and M. Gomina, "Optimizing the formulation of flax fiber-reinforced cement composites," *Constr. Build. Mater.,* vol. 54, p. 659–664, 2014, doi:10.1016/j.conbuildmat.2013.12.038.

[62] P. F. De Aguiar, B. Bourguignon, M. S. Khots, D. L. Massart and R. Phan-Than-Luu, "D-optimal designs," *Chemom. Intell. Lab. Syst.,* vol. 30, p. 199–210, 1995, doi:10.1016/0169-7439(94)00076-X.

[63] P. Krajnik, J. Kopac and A. Sluga, "Design of grinding factors based on response surface methodology," *J. Mater. Process. Technol.,* vol. 162–163, p. 629–636, 2005, doi:10.1016/j.jmatprotec.2005.02.187.

[64] G. E. Box, J. Stuart Hunter and W. G. Hunter, Statistics for experimenters: design, innovation, and discovery, John Wiley and sons, 2005, ISBN-13: 978-0471718130 , p. 629.

[65] Software for design of experiments and optimization, Umetrics: http://www.umetrics.com, 2016.

[66] B. Li, A. J. Morris and E. B. Martin, "Generalized partial least squares regression based on the penalized minimum norm projection," *Chemom. Intell. Lab. Syst.,* vol. 72, p. 21–26, 2004, doi:10.1016/j.chemolab.2004.01.026.

[67] S. Bouzalakos, A. W. Dudeney and B. K. Chan, "Formulating and optimising the compressive strength of controlled low-strength materials containing mine tailings by mixture design and response surface methods," *Miner. Eng.,* vol. 53, p. 48–56, 2013, doi:10.1016/j.mineng.2013.07.007.

[68] J. Goupy, Plans d'expériences : les mélanges, Paris: DUNOD, 2001, p. 285.

[69] R. A. Fisher, The design of experiments, New York, Hafner: Libraries Australia, 1971, p. 248.

[70] J. Biarez and P. Y. Hicher, Elementary mechanics of soil behaviour: saturated remoulded soils, A.A. Balkema, Amsterdam, Netherlands, 1994, ISBN 90-5410-156-3 (rel.). - ISBN 90-5410-157-1 (br.).

[71] Y. Brouard, N. Belayachi, D. Hoxha, N. Ranganathan and S. Méo, "Mechanical and hygrothermal behavior of clay – Sunflower (Helianthus annuus) and rape straw (Brassica napus) plaster bio-composites for building insulation," *Constr. Build. Mater.,* vol. 161, p. 196–207, 2018, doi:10.1016/j.conbuildmat.2017.11.140.

[72] A. Beukers, Lightness. The inevitable renaissance of minimum energy structure, Rotterdam: v. Hinte, 1998.

[73] R. A. Fisher, Statistical methods, experimental design, and scientific inference: a re-issue of statistical methods for research workers, the design of experiments, and statistical methods and scientific inference, New York: Hafner publishing company, 1995, p. 323.

[74] D. Gallipoli, A. W. Bruno, C. Perlot and J. Mendes, "A geotechnical perspective of raw earth building," *Acta Geotech.,* vol. 12, p. 463–478, 2017, doi:10.1007/s11440-016-0521-1.

593

594

Figure captions

Table captions:

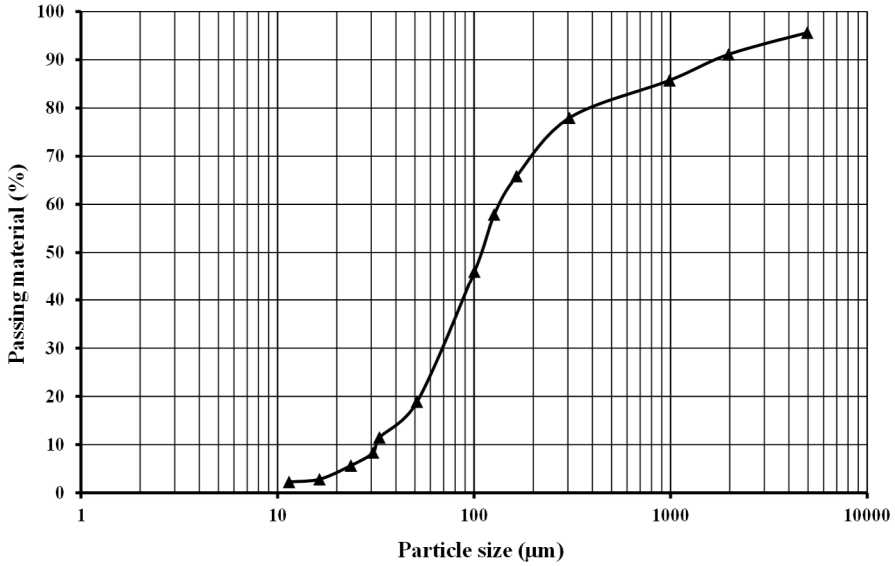

Fig.1: Silt grading size distribution curve

Fig.2: Vegetal flax fibers

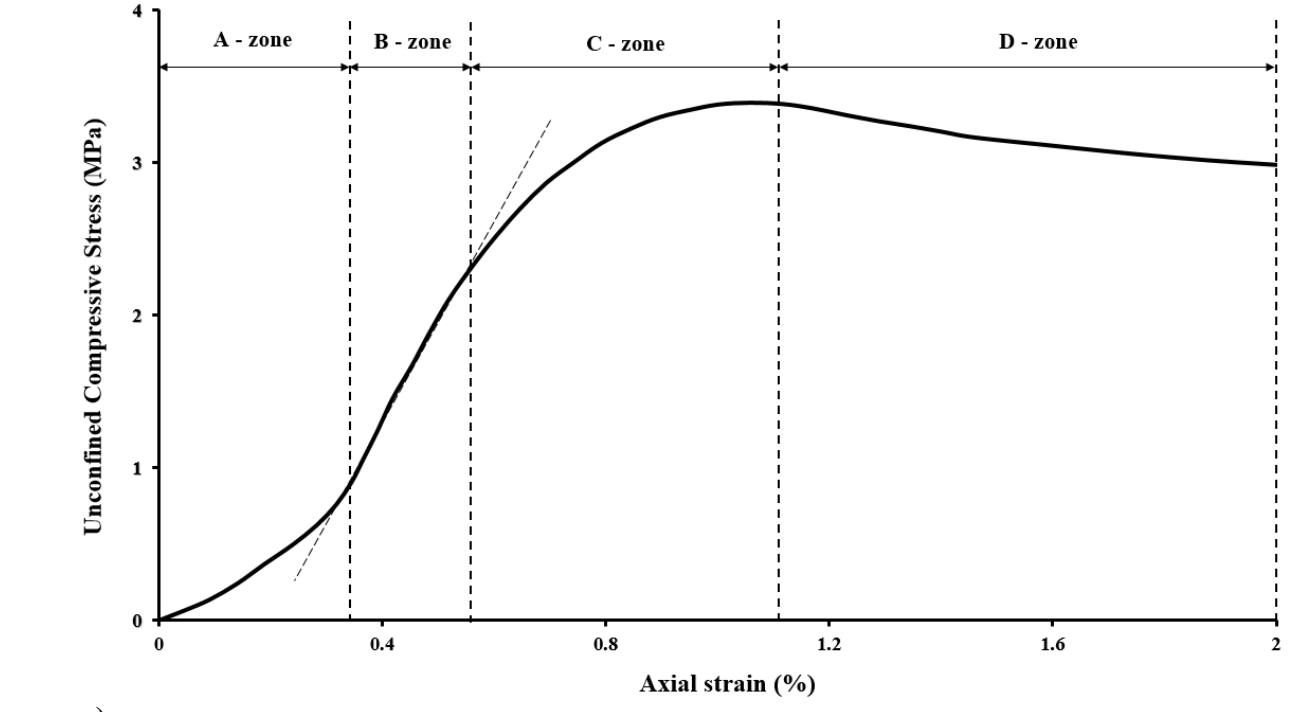

a)

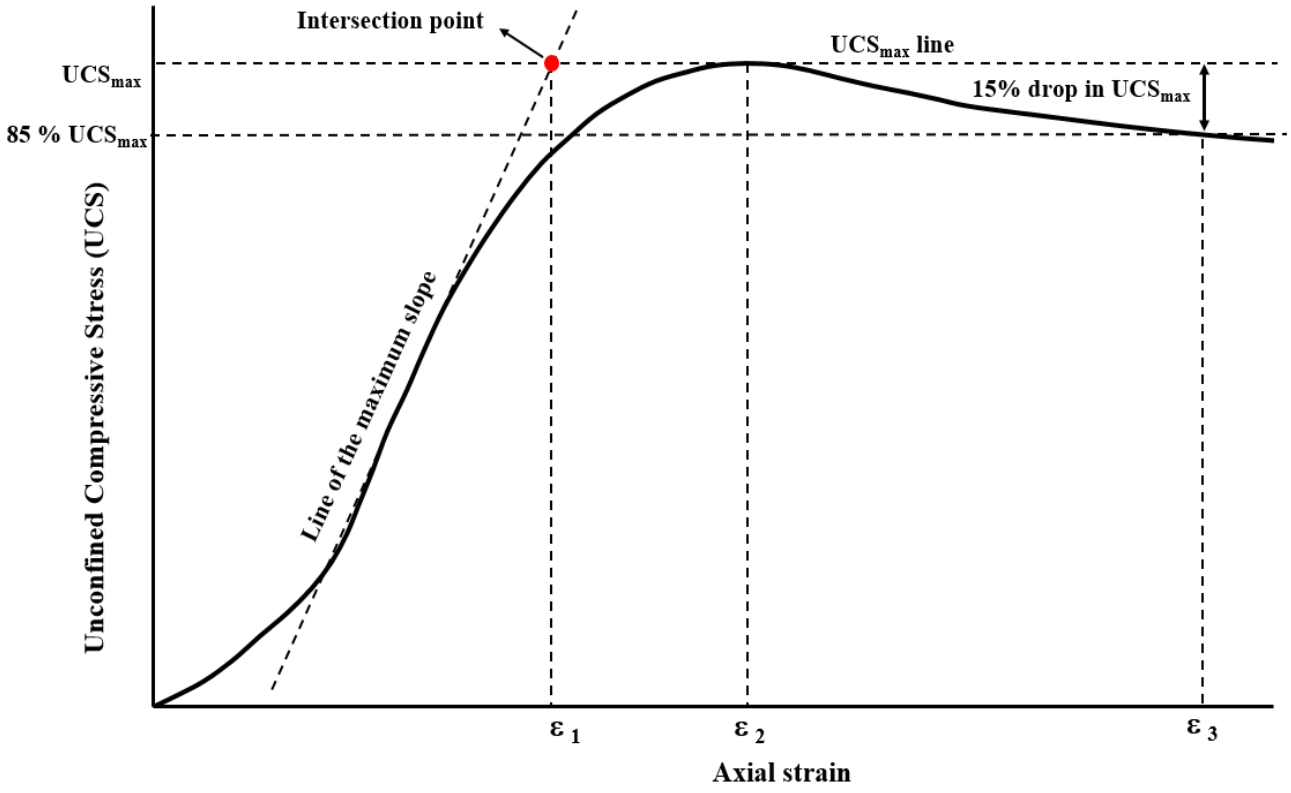

b)

Fig. 3: a) UCS stress-strain curve for formulation F9 after 90-days of curing time with the identification of four zones, b) Ductility indices definitions ($i = \frac{\varepsilon_3}{\varepsilon_1}$, $i' = \frac{\varepsilon_3}{\varepsilon_2}$)

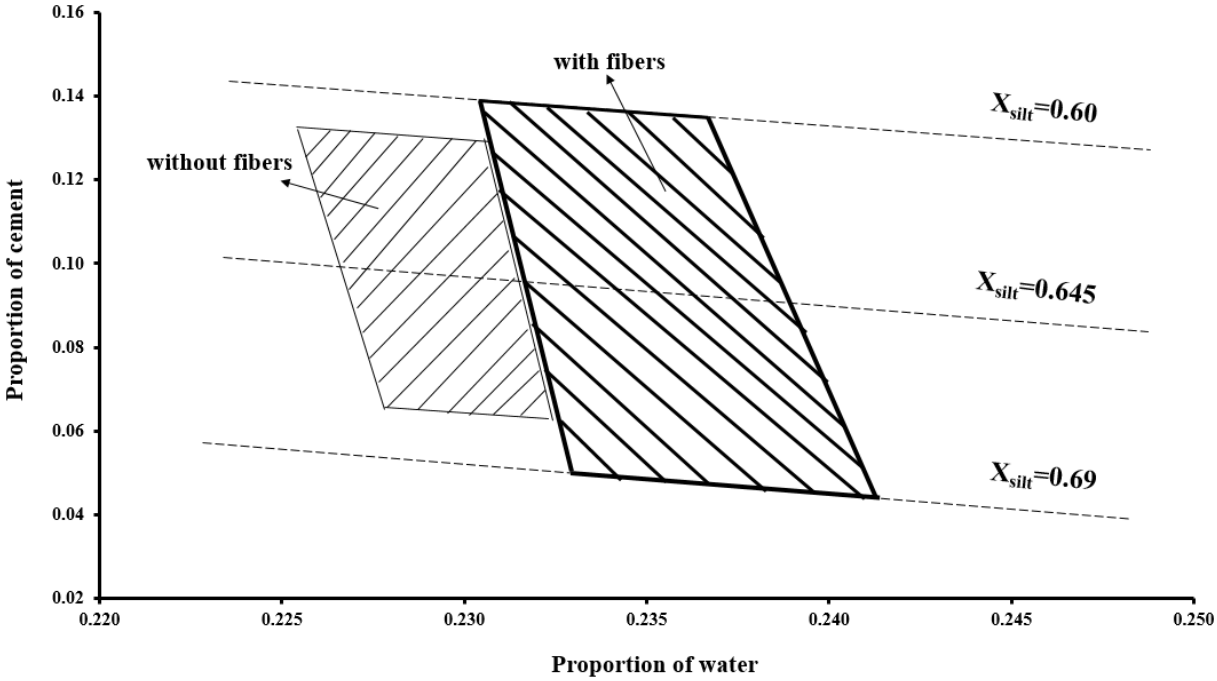

Fig. 4: Projection in the (X_{cement}, X_{water}) plane of the experimental region validating the workability condition (dashed regions) for mixtures without fibers (Eq. 4, [4]) and with fibers (Eq. 3). X_{cement} and X_{water} are respectively the proportions of cement and water. The proportion of lime is fixed to X_{lime} =0.02. Dashed lines: Isovalues of X_{silt} proportion.

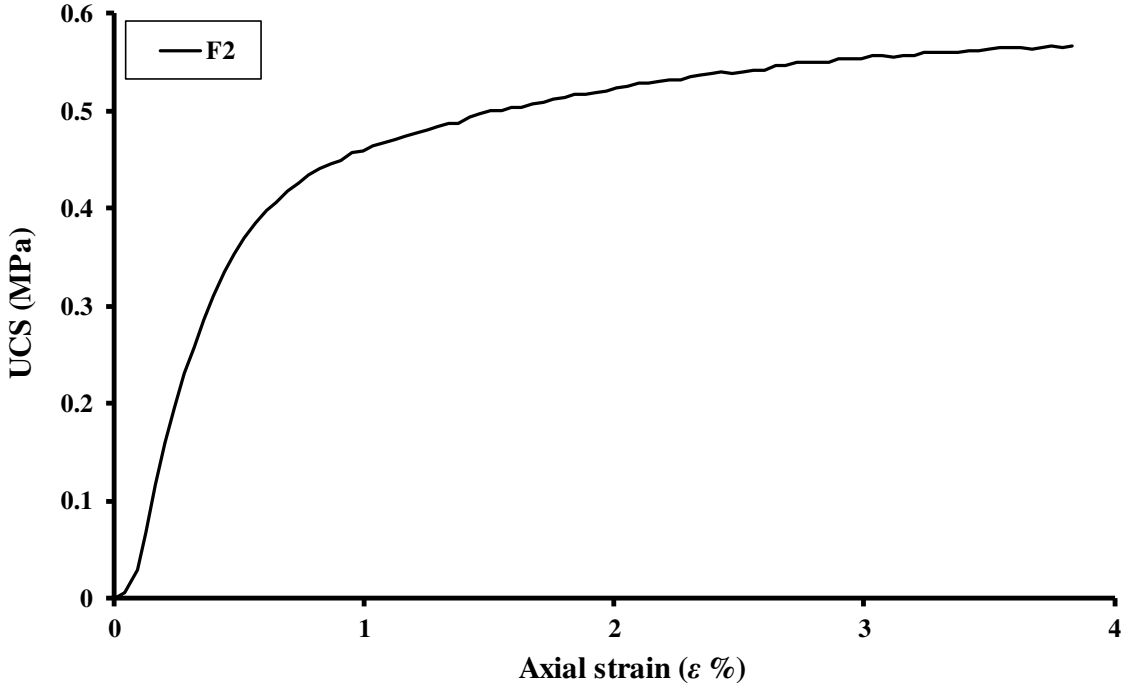

Fig. 5: Unconfined Compressive Stress (UCS) as a function of the axial strain for formulation F2

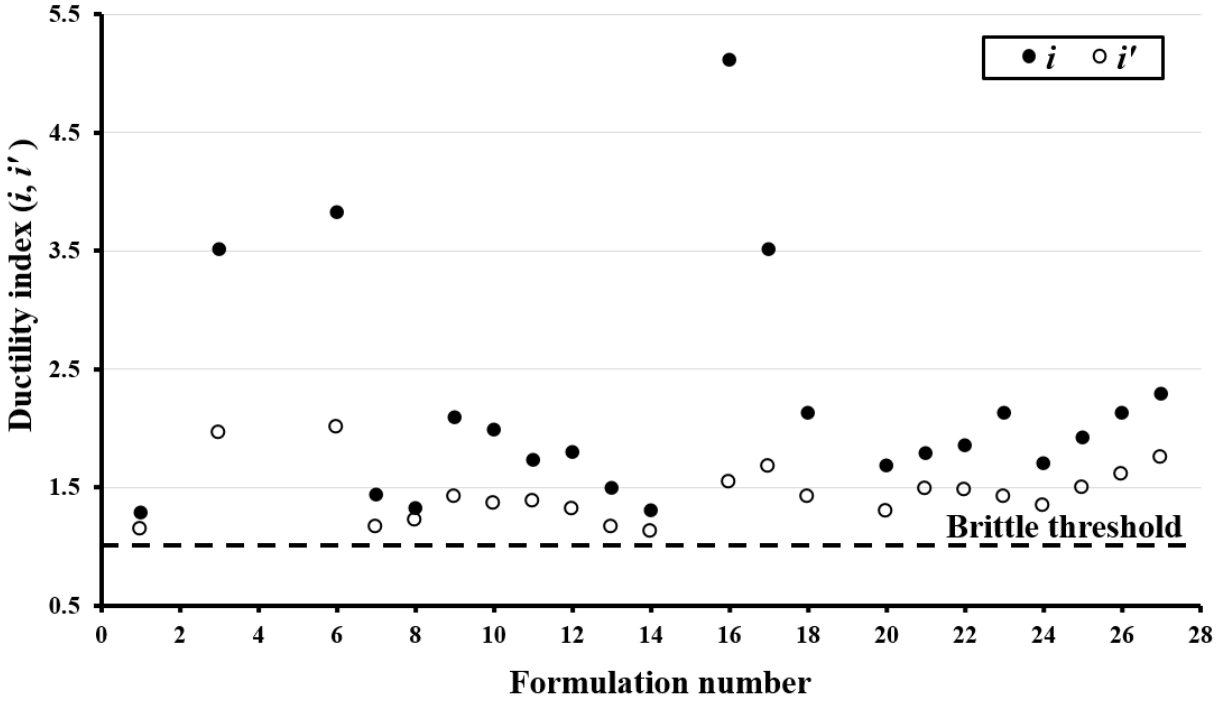

Fig. 6: Ductility indices versus formulation number

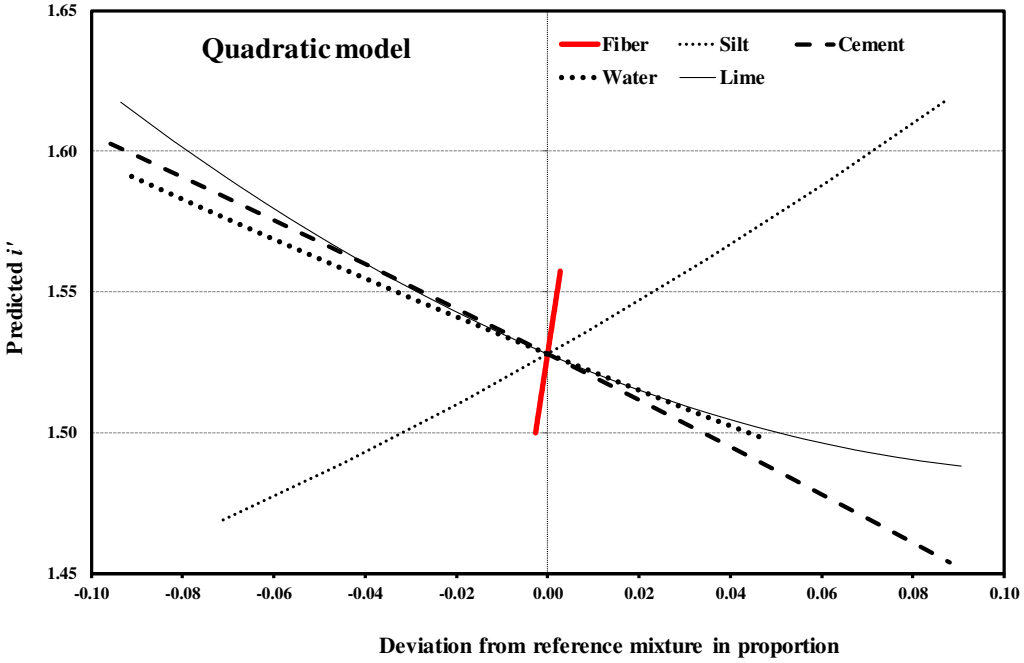

a)

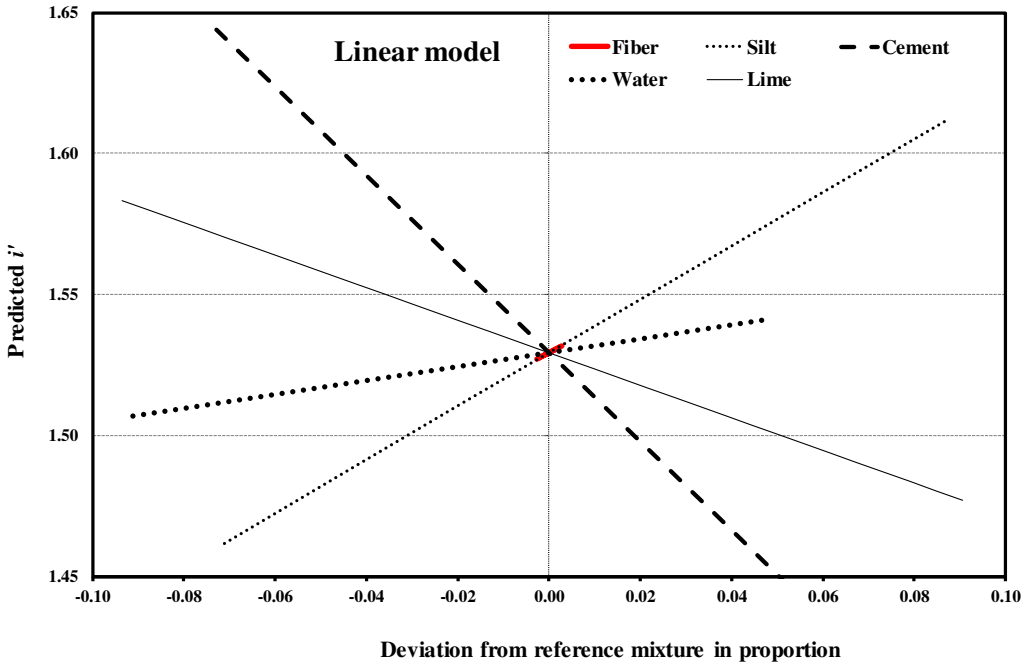

b)

Fig. 7: Response trace plots of ductility index i' a) quadratic model, b) linear model

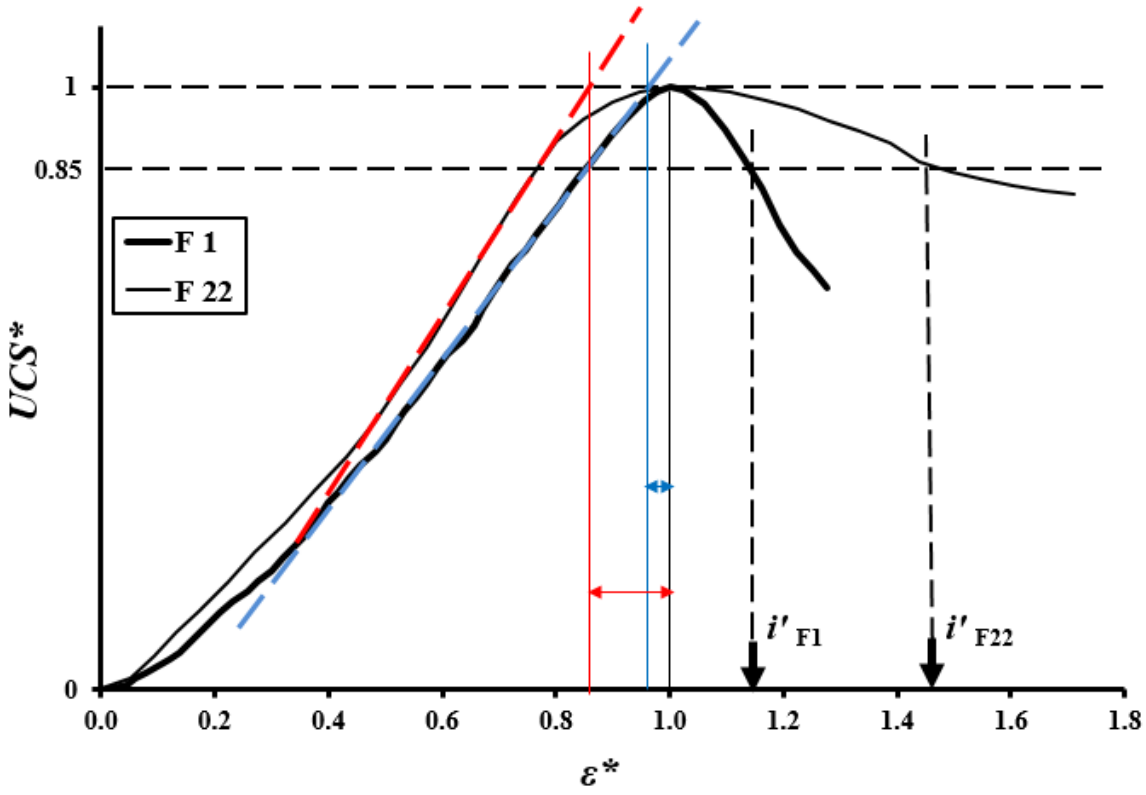

Fig. 8: Normalized stress-strain curve for the two formulations F1 and F22

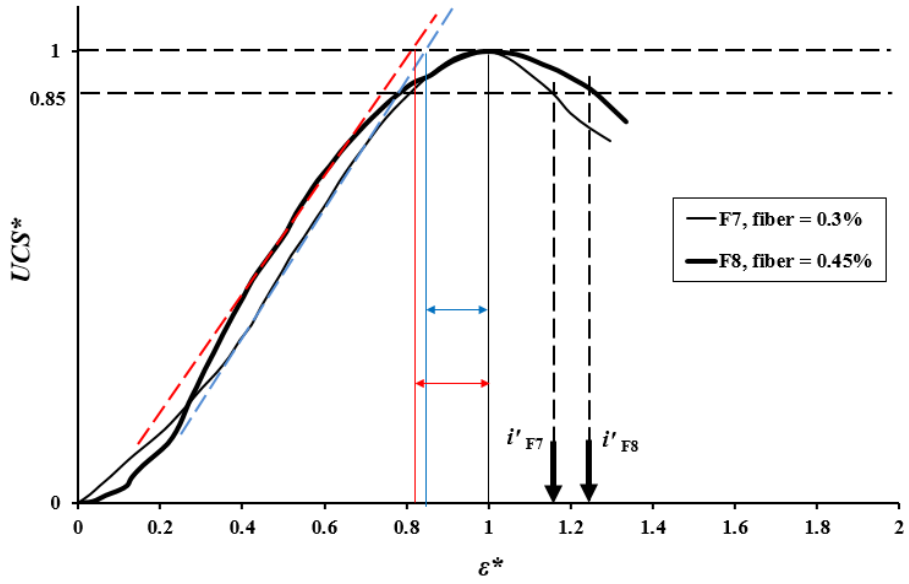

a)

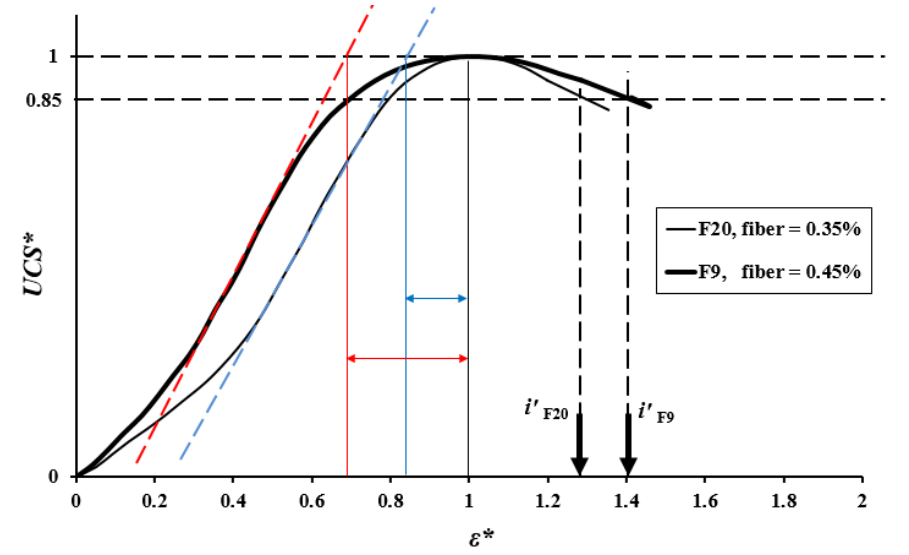

b)

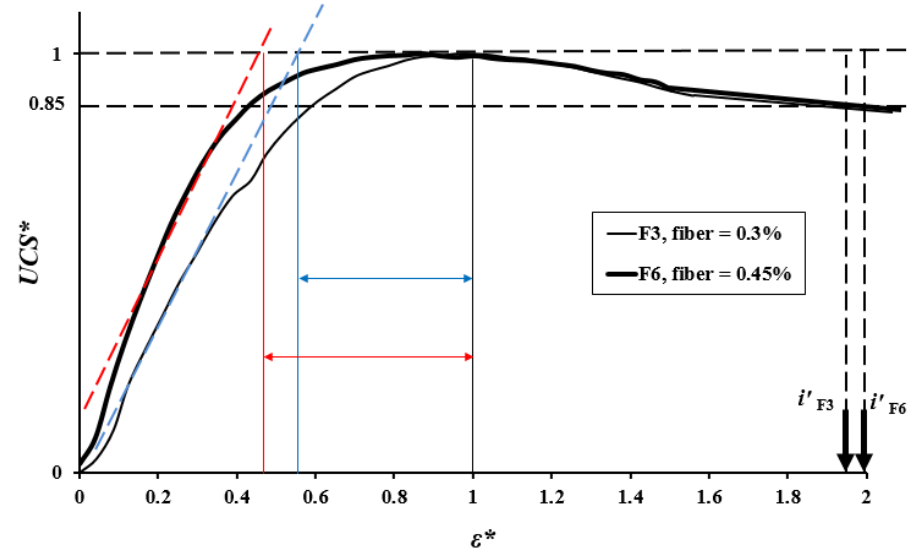

c)

Fig. 9: Normalized stress-strain curve for formulations almost similar except by the fiber content

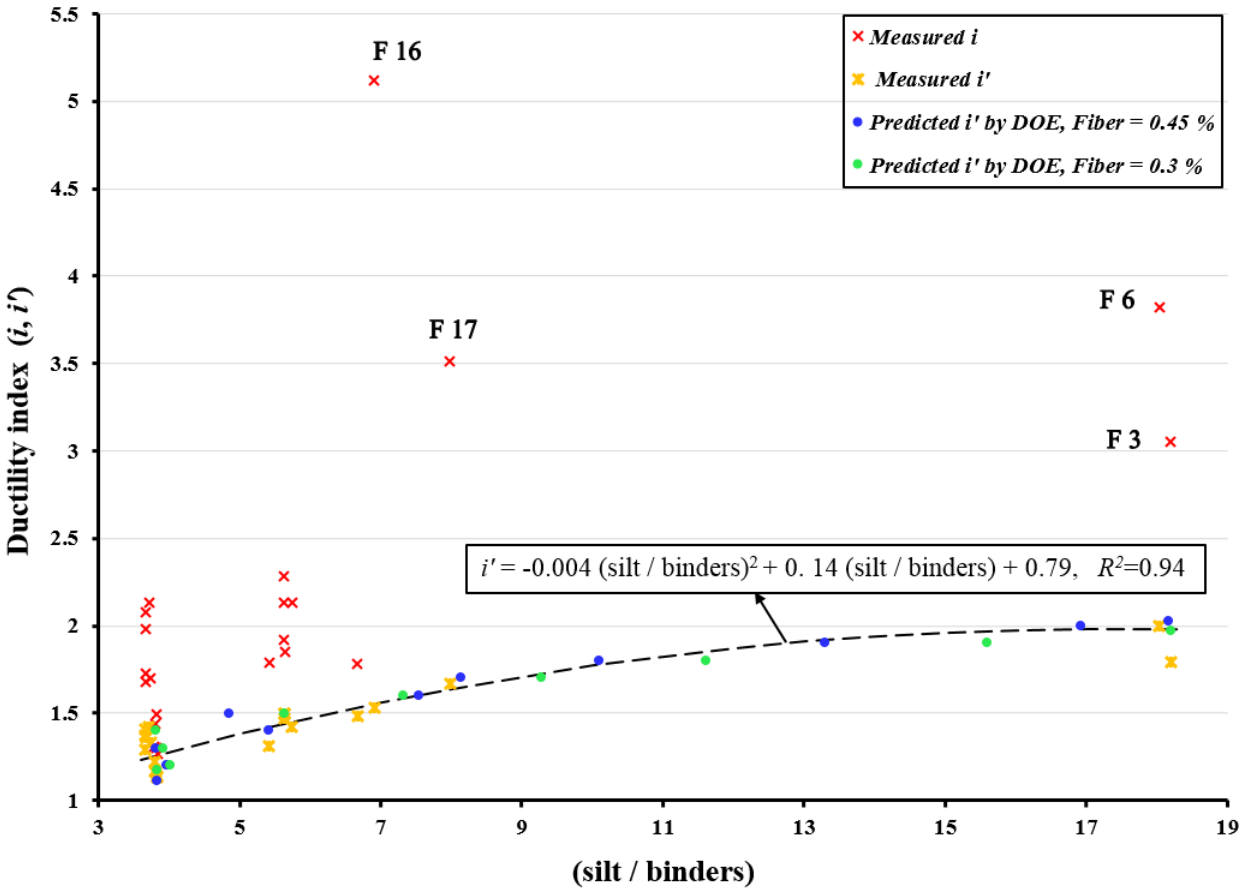

Fig. 10: Ductility indices as a function of the silt/binders ratio

Table 1: Mechanical and physical properties of vegetal flax fibers ([47], [72])

Parameters	
Density $\rho_{\text{fiber}}/\rho_{\text{water}}$	1.4
Fiber diameter d (μm)	10-15
Young's modulus E (GPa)	40-85
Failure stress σ_u (MPa)	800-2000
Failure strain ε_u (%)	2.4-3.3

Table 2: Mixing range

x_i	Lower limit (%)	Upper limit (%)
x_1: Fiber	0.3	0.45
x_2: Lime	0	12
x_3: Cement	4	16
x_4: Water	20	25
x_5: Silt	47	75

Table 3: Experimental design of the D-optimal design for a raw earth concrete

Formulation	Fiber (x_1)	Lime (x_2)	Cement (x_3)	Water (x_4)	Silt (x_5)	Ductility index *i*	Ductility index *i'*
1	0.0030	0.0000	0.1600	0.2239	0.6131	1.27	1.14
2	0.0030	0.0647	0.0400	0.2500	0.6423	-	-
3	0.0030	0.0000	0.0400	0.2290	0.7280	3.51	1.96
4	0.0045	0.0000	0.0400	0.2287	0.7268	-	-
5	0.0030	0.0000	0.0400	0.2345	0.7225	-	-
6	0.0045	0.0000	0.0400	0.2342	0.7213	3.82	2.00
7	0.0030	0.0000	0.1600	0.2295	0.6075	1.44	1.17
8	0.0045	0.0000	0.1600	0.2292	0.6063	1.31	1.22
9	0.0045	0.0719	0.0881	0.2500	0.5855	2.08	1.41
10	0.0030	0.0560	0.1040	0.2500	0.5870	1.98	1.36
11	0.0045	0.0568	0.1032	0.2500	0.5855	1.73	1.37
12	0.0045	0.0000	0.1200	0.2253	0.6502	1.79	1.31
13	0.0045	0.0000	0.1600	0.2255	0.6100	1.49	1.16
14	0.0040	0.0000	0.1600	0.2237	0.6123	1.30	1.13
15	0.0030	0.0237	0.1363	0.2326	0.6044	-	-
16	0.0045	0.0543	0.0400	0.2500	0.6512	5.12	1.53
17	0.0045	0.0438	0.0400	0.2429	0.6688	3.51	1.67
18	0.0045	0.0479	0.1121	0.2412	0.5943	2.13	1.42
19	0.0035	0.0480	0.0400	0.2500	0.6585	-	-
20	0.0035	0.0713	0.0887	0.2500	0.5865	1.68	1.29
21	0.0038	0.0000	0.1000	0.2291	0.6672	1.78	1.48
22	0.0030	0.0299	0.0841	0.2396	0.6433	1.85	1.47
23	0.0038	0.0261	0.0859	0.2409	0.6433	2.13	1.42
24	0.0038	0.0320	0.1280	0.2383	0.5980	1.70	1.33
25	0.0038	0.0301	0.0840	0.2395	0.6426	1.92	1.50
26	0.0038	0.0301	0.0840	0.2395	0.6426	2.13	1.60
27	0.0038	0.0301	0.0840	0.2395	0.6426	2.28	1.50

Table 4: The coefficients of the linear and quadratic models for i and i' ductility indices for 90-days of curing time

Coefficients	Quadratic model, *i*	Quadratic model, *i'*	Linear model, *i*	Linear model, *i'*
a_0	35.00	0.41	2.48	-0.71
a_1	-5321.80	-504.08	254.05	4.60
a_2	-2.71	54.77	-7.95	-0.14
a_3	151.13	-5.74	-20.78	-2.98
a_4	-174.68	-6.21	4.52	2.39
a_5	-43.99	5.38	-0.08	2.97
a_{12}	4507.81	321.78	-	-
a_{13}	-5379.10	-369.63	-	-
a_{14}	17838.80	1900.83	-	-
a_{15}	2862.35	168.07	-	-
a_{23}	-2.69	42.04	-	-
a_{24}	-87.11	-218.54	-	-
a_{25}	15.34	-13.30	-	-
a_{34}	-198.25	92.14	-	-
a_{35}	-146.26	-27.75	-	-
a_{45}	228.84	-5.10	-	-

Table 5: Values of R^2, R^2_{adj} and Q^2

Ductility index	Linear model	Quadratic model
i	R^2=0.74, R^2_{adj}=0.68, Q^2=0.60	R^2=0.84, R^2_{adj}=0.43, Q^2=0.35
i'	R^2=0.86, R^2_{adj}=0.81, Q^2=0.77	R^2=0.92, R^2_{adj}=0.73, Q^2=0.84

Table 6: ANOVA Table for i' ductility index

Source of variation	Degrees of Freedom (DF)	Sum of Squares (SS)	Mean Square (MS)	F-value	P-value
Quadratic model					
Regression	15	1.131	0.075	4.688	0.032
Residual error	6	0.094	0.016		
Lack-of-fit	4	0.063	0.016	0.99	0.558
Pure error	2	0.032	0.016		
Total	21	1.225	0.058		

Table 7: First F-Test (model significance test: $(\text{F-value})_{\text{critical}} < (\text{F-value})_{\text{model}}$)

Model	F-value (critical)	F-value (model)
Quadratic model for i' ductility index	3.940	4.688

Table 8: Second F-Test ($(\text{F-value})_{\text{critical}} > (\text{F-value})_{\text{LOF}}$)

Model	F-value (critical)	F-value (LOF)
Quadratic model for i' ductility index	19.2	0.99

Table 9: Deduced values of i' and $\varepsilon_1/\varepsilon_{max}$ from Fig. 9

Fig. 9	0.35% fibers		0.45% fibers	
	i'	$\varepsilon_1/\varepsilon_{max}$	i'	$\varepsilon_1/\varepsilon_{max}$
Fig. 9 a	*1.17*	0.83	1.22	0.82
Fig. 9 b	1.29	0.82	1.41	0.69
Fig. 9 c	1.96	0.55	2	0.49